

Universal correlation for the rise velocity of long gas bubbles in round pipes

By FLAVIA VIANA¹, RAIMUNDO PARDO¹,
RODOLFO YÁNEZ¹, JOSÉ L. TRALLERO¹
AND DANIEL D. JOSEPH²

¹PDVSA-Intevap. Los Teques, Edo. Miranda, 1201. Venezuela

²Department of Aerospace Engineering and Mechanics, University of Minnesota, Minneapolis, MN 55455, USA

(Received 23 July 2002 and in revised form 8 August 2003)

We collected all of the published data we could find on the rise velocity of long gas bubbles in stagnant fluids contained in circular tubes. Data from 255 experiments from the literature and seven new experiments at PDVSA Intevap for fluids with viscosities ranging from 1 mPa s up to 3900 mPa s were assembled on spread sheets and processed in log–log plots of the normalized rise velocity, $Fr = U/(gD)^{1/2}$ Froude velocity vs. buoyancy Reynolds number, $R = (D^3 g(\rho_l - \rho_g)\rho_l)^{1/2}/\mu$ for fixed ranges of the Eötvös number, $EO = g\rho_l D^2/\sigma$ where D is the pipe diameter, ρ_l , ρ_g and σ are densities and surface tension. The plots give rise to power laws in EO ; the composition of these separate power laws emerge as bi-power laws for two separate flow regions for large and small buoyancy Reynolds. For large R (>200) we find

$$Fr = 0.34/(1 + 3805/EO^{3.06})^{0.58}.$$

For small R (<10) we find

$$Fr = \frac{9.494 \times 10^{-3}}{(1 + 6197/EO^{2.561})^{0.5793}} R^{1.026}.$$

The flat region for high buoyancy Reynolds number and sloped region for low buoyancy Reynolds number is separated by a transition region ($10 < R < 200$) which we describe by fitting the data to a logistic dose curve. Repeated application of logistic dose curves leads to a composition of rational fractions of rational fractions of power laws. This leads to the following universal correlation:

$$Fr = L[R; A, B, C, G] \equiv \frac{A}{(1 + (R/B)^C)^G}$$

where

$$A = L[EO; a, b, c, d], \quad B = L[EO; e, f, g, h], \quad C = L[EO; i, j, k, l], \quad G = m/C$$

and the parameters (a, b, \dots, l) are

$$a=0.34; \quad b=14.793; \quad c=-3.06; \quad d=0.58; \quad e=31.08; \quad f=29.868; \quad g=-1.96; \\ h=-0.49; \quad i=-1.45; \quad j=24.867; \quad k=-9.93; \quad l=-0.094; \quad m=-1.0295.$$

The literature on this subject is reviewed together with a summary of previous methods of prediction. New data and photographs collected at PDVSA-Intevap on the rise of Taylor bubbles is presented.

1. Literature review

Readers not familiar with Taylor bubbles should look at the photographs shown in figure 5 below. These bubbles almost fill the tube cross-section and lead to the formation of a falling film between the wall and the bubble. They also exhibit a rounded nose and in water give rise to an unsteady and irregular tail. We follow the convention introduced by previous authors who use the words ‘Taylor bubble’ to describe the rise of long gas bubbles in circular tubes. Further information is given in the excellent treatise of Wallis (1969). An early review of literature on the rise velocity of Taylor bubbles in round pipes is given by Rader, Bourgoyne & Ward (1975), Clift, Grace & Weber (1978) and Fabr e & Lin e (1992). The review given here updates the recent review of Viana *et al.* (2001).

Research on Taylor bubbles dates back as far as 1913 to that by Gibson (cited by White & Beardmore 1962). Later, this subject was addressed by Dumitrescu (1943) and Davies & Taylor (1950). Both papers pointed out that a gas bubble must assume a shape that allows the surface of the bubble to be an isobar.

The papers by Dumitrescu (1943), Davies & Taylor (1950), Brown (1965), White & Beardmore (1962), Zukoski (1966) and the textbook of Wallis (1969) give prediction formulae for the rise velocity. The first three use models and analysis to make their predictions, the last three obtain predictions from processing data. Dumitrescu (1943) computed the approximate shape of a bubble rising in a vertical tube from theoretical considerations. The computed profile had a rounded nose and resembled a bullet. Davies & Taylor also published photographs showing that a bubble rising in a circular tube was bullet shaped. By ignoring the frictional and capillary effects, and by considering only the potential and kinetic energy of the liquid falling around the bubble, the approximate solution for the liquid flow around the top of the bubble was determined by both Dumitrescu and Davies & Taylor. The solution published by Dumitrescu relates the bubble velocity U through a liquid in a vertical circular tube to the tube diameter and the acceleration due to gravity by the following equation:

$$U = 0.351\sqrt{Dg} \text{ (circular tube)}. \quad (1)$$

This equation generally agreed with the equation later presented by Davies & Taylor, which contained the constant 0.328 in place of the constant 0.351 in (1). However, as shown in tables A1 and A2 in the Appendix†, experimental data obtained by several investigators using air and water indicate that the equation presented by Dumitrescu applies best in the larger tubes.

Davies & Taylor (1950) also analysed the related problem of the rise of a spherical cap bubble in an unbounded liquid without the restraining effect of tube walls. They found the value $\sqrt{2/3}$ instead of the lower value 0.328 for long gas bubbles associated with the effects of liquid drainage on the tube walls. There are a number of anomalous features associated with the rise of long bubbles in tubes and spherical cap bubbles which have yet to be explained by the principles of fluid mechanics. These anomalies will be discussed in §6.

Laird & Chisholm (1956) also investigated bubble rise velocity through water in vertical tubes. Working with a 2 in. diameter tube, they found bubble rise velocities similar to those of Davies & Taylor. However, Laird & Chisholm reported a 10% increase in bubble rise velocity as the length of the bubble was increased from 2 to

† Available as a supplement to the online version of this paper, or from the authors or the JFM Editorial Office, Cambridge.

25 pipe diameters. Since (1) does not contain a bubble-length term, this observation and the measurements suggest that the rise velocity is nearly independent of length when the bubble length is more than a few pipe diameters.

Griffith & Wallis (1961) investigated experimentally the two-phase slug flow through various sizes of round pipes. Some of their experiments were done with single Taylor bubbles rising in stagnant water. The measured rise velocities were in agreement with the prediction of Dumitrescu (1). Regarding the applicability of (1) to finite bubbles, Griffith & Wallis stated '... the finiteness of the slug flow bubbles did not appear to make much difference in their rise velocity.'

White & Beardmore (1962) presented extensive experimental data on the rise of Taylor bubbles in several different stagnant liquids. They used their own and literature data to propose a general graphical correlation for predicting the terminal rise velocity of bubbles in round pipes. They noted that '... for cylindrical bubbles the terminal velocity is practically independent of the length of the bubble,' in agreement with previous works. White & Beardmore recognized the effect of the bubble expansion as it rises into a lower hydrostatic pressure on the measured values on the rise velocity.

A correlation of data presented in graphs given by White and Beardmore was developed and is

$$U = \sqrt{gD} \left(\frac{a_1 a_2 \exp(a_3 t)}{a_1 + a_2 (\exp(a_3 t) - 1)} - a_4 \right) \quad (2)$$

where

$$t = \log_{10} \left(\frac{\rho_l g D^2}{\sigma} \right), \quad (3)$$

and σ is surface tension.

The parameters a_i in (2) are seventh-degree polynomials:

$$a_i = \sum_{j=1}^8 c_{ij} x^{j-1} \quad (i = 1, \dots, 4), \quad (4)$$

$$x = \log_{10} \left(\frac{g\mu^4}{\rho_l \sigma^3} \right). \quad (5)$$

where μ is liquid viscosity and the coefficients c_{ij} are

$$c_{ij} = \begin{bmatrix} 3.5603852 \times 10^{-1} & 2.6717658 \times 10^{-3} & -2.7121907 \times 10^{-3} & -2.0001955 \times 10^{-3} \\ 1.5642441 \times 10^{-3} & 2.8532721 \times 10^{-4} & -4.7831508 \times 10^{-5} & -3.605927 \times 10^{-5} \\ 3.059819 & -5.2353564 \times 10^{-1} & 3.3906415 \times 10^{-2} & 2.1368428 \times 10^{-2} \\ 2.3221312 \times 10^{-2} & -1.809746 \times 10^{-3} & 9.3468732 \times 10^{-5} & -2.3440168 \times 10^{-4} \\ 8.622533 \times 10^{-5} & 5.7198751 \times 10^{-5} & -2.4316663 \times 10^{-6} & -6.7582431 \times 10^{-7} \\ 7.6382727 \times 10^{-6} & 1.1736259 \times 10^{-6} & -1.5186036 \times 10^{-7} & -1.9756221 \times 10^{-8} \\ -3.2676237 \times 10^{-3} & -7.302379 \times 10^{-4} & 7.2215493 \times 10^{-5} & 1.1273658 \times 10^{-5} \\ 5.9716008 \times 10^{-5} & 9.7852173 \times 10^{-6} & -1.3514105 \times 10^{-6} & -1.74642 \times 10^{-7} \end{bmatrix}.$$

White & Beardmore referred to the dimensionless parameter $g\mu^4/\rho_l\sigma^3$ in (5) as the property group (Y). Clift *et al.* (1978) called this group the Morton number (M).

The correlation (2) has the limits

$$5 < Eo < 1000, \quad 10^{-8} < Y < 10^6,$$

where Eötvös number $Eo = g\rho_l D^2/\sigma$.

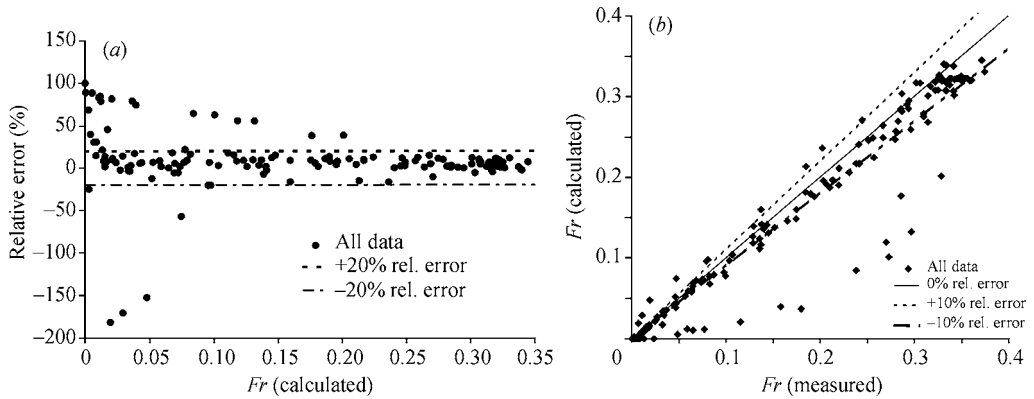


FIGURE 1. (a) Relative error plot, (b) measured vs. calculated Fr using (2)–(5). These plots show an overall good performance for White & Beardmore’s correlation, except for some data for which we were unable to find an explanation.

The performance of White & Beardmore’s model using the data in the Appendix is presented in figure 1. This model yielded a rather high squared residuals sum of Froude number $Fr = U/(gD)^{1/2}$:

$$\sum (Fr_{meas.} - Fr_{calc.})^2 = 0.23$$

when tested against the data.

Goldsmith & Mason (1962) presented a simple model for the hydrodynamics of large bubbles and liquid drops, taking into account the liquid viscosity. Also, they included the results of an extensive experimental investigation for bubbles and liquid drops rising or falling in a small diameter round tube with suspending liquids with several physical properties. Among many valuable observations is that for a constant value of Eu , the overall bubble deformation (nose, film and tail) remained independent of the liquid viscosity μ .

The issue of the dependence of rise velocity and bubble length, which is not directly addressed by (1) or (2), was further investigated by Nicklin, Wilkes & Davidson (1962). They measured the rise velocity of Taylor bubbles of several lengths using different experimental arrangements in order to isolate the secondary effects due to bubble expansion. Nicklin *et al.* arrived at the conclusion that (1) accurately predicted the rise velocity of the Taylor bubbles studied in their experiments. Regarding the bubble expansion effect, they stated, ‘This (rise) velocity is independent of the slug (Taylor bubble) length, and is modified only by a net flow of liquid across a section above the slug’. They also proposed that: (a) ‘... the slug (Taylor bubble) can be assumed to consist of a nose region in which the liquid accelerates freely under gravity, and a lower region in which gravity is balanced by wall shear forces and the film thickness is constant,’ and (b) ‘It is therefore a correct generalization to say that slugs always tend to rise as quickly as possible’.

Brown (1965) made an experimental and theoretical study of the effect of liquid viscosity in the terminal rise velocity of Taylor bubbles. Brown stated that the potential flow solution (e.g (1)) described quite well the velocities of bubbles in liquids of low viscosities, but it was not suitable for liquids with higher viscosities. Through some experiments, Brown found that regardless the viscosity of the liquid, the noses of the different Taylor bubbles tested showed geometric similarity, in agreement with

Goldsmith & Mason's findings. This led Brown to propose a more general form of (1) including the retarding effect of the liquid viscosity. This effect was taken into account through the analysis of the falling liquid film thickness well below the bubble's nose. The original form of Brown's equation is

$$U = 0.35\sqrt{gD}\sqrt{1 - 2\left(\frac{\sqrt{1 + ND} - 1}{ND}\right)} \tag{6}$$

where

$$N = \left(14.5\frac{\rho_l^2 g}{\mu^2}\right)^{1/3} \tag{7}$$

N is dimensional but ND is dimensionless.

The applicability limits of (6) were established empirically as

$$\begin{aligned} \text{surface tension: } & \frac{\rho_l g D^2}{4\sigma} \left(1 - 2\left(\frac{\sqrt{1 + ND} - 1}{ND}\right)\right)^2 > 5.0, \\ \text{viscosity: } & ND > 60. \end{aligned}$$

Zukoski (1966) performed an extensive experimental study of the relevant variables influencing the rise velocity of Taylor bubbles: viscosity, density, surface tension, pipe diameter and angle of inclination. This work is perhaps the most comprehensive available in the literature. Zukoski took data available in the literature along with own data and used a set of three dimensionless parameters to analyse them. These parameters are: Reynolds number, $R_z = \rho_l U D / (2\mu)$, dimensionless velocity, $Fr_z = U / (gD/2)^{1/2}$ and the surface tension number, $\Sigma = 4\sigma / (\rho_l g D^2)$. It was observed that '... for Reynolds number greater than about 200, the propagation rates are substantially independent of viscous effects'. This implies that the bubble's movement is governed solely by Σ . Also, for $\Sigma < 0.1$, the rise velocity is almost equal to that predicted by (1). The different effects of viscosity and surface tension upon the rise velocity are combined using

$$Fr_z(R_z, \Sigma) = Fr_z(\infty, \Sigma)f(R_z) \tag{8}$$

A numerical form of $Fr_z(\infty, \Sigma)$ and $f(R_z)$ was obtained fitting the data points displayed in Zukoski's paper:

$$Fr_z(\infty, \Sigma) = 0.4664 + 0.3473\Sigma - 5.3928\Sigma^2 + 10.532\Sigma^3 - 6.7095\Sigma^4 \quad (\Sigma < 0.6), \tag{9}$$

$$f(R_z) = \frac{1}{(1 + 44.72/R_z^{1.8})^{0.279}} \tag{10}$$

For a given set of physical properties and pipe radius, the bubble's rise velocity can be calculated through a numerical method using (8), (9) and (10). Note that $R_z = R Fr/2$ and $\Sigma = 4/Eo$. The performance of Zukoski's model using the data in the Appendix is presented in figure 2. The sum of squared residuals for this model is 0.07.

Wallis (1969) proposed a general correlation for Taylor bubble rise velocity in terms of all the relevant variables:

$$U = k \left[\frac{Dg(\rho_l - \rho_g)}{\rho_l} \right]^{1/2} \tag{11}$$

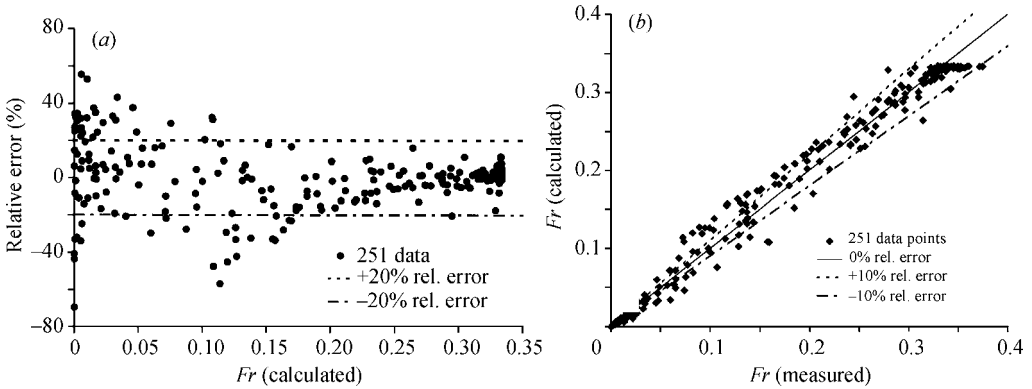


FIGURE 2. (a) Relative error plot for Zukoski's correlation. Only 251 experiments were included with $Eo > 7$. (b) Measured vs. calculated Fr .

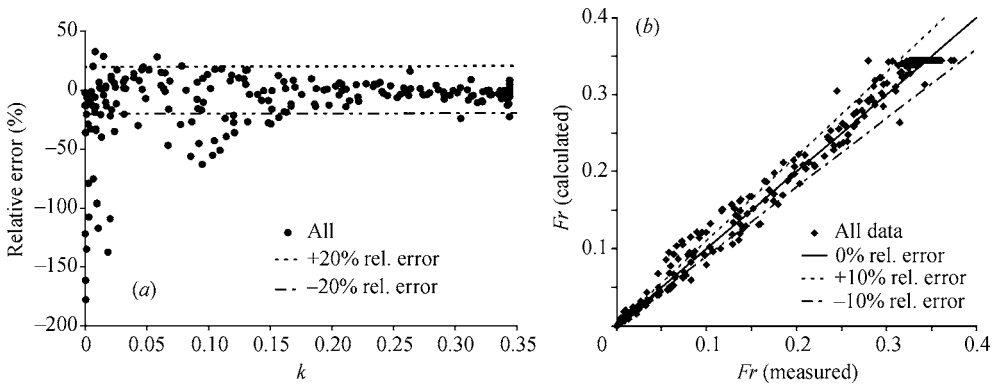


FIGURE 3. (a) Residuals plot for Wallis's correlation, (b) measured vs. calculated Fr .

and

$$k = 0.345(1 - e^{-0.01R/0.345})(1 - e^{(3.37 - Eo)/m}), \tag{12}$$

where R is the buoyancy Reynolds number:

$$R = \frac{[D^3 g(\rho_l - \rho_g)\rho_l]^{1/2}}{\mu}; \tag{13}$$

m is a function of R and takes on the following values:

$$\left. \begin{aligned} R > 250: & \quad m = 10, \\ 18 < R < 250: & \quad m = 69R^{-0.35}, \\ R < 18: & \quad m = 25. \end{aligned} \right\} \tag{14}$$

The performance of Wallis's correlation can be seen in figure 3. The sum of squared residuals is 0.06.

Tung & Parlange (1976) studied long gas bubbles rising in closed cylindrical tubes of large diameter in which viscosity effects are suppressed (Reynolds number of the flow based on the radius of the tube is larger than 50) and surface tension effects could be isolated. An analytical solution is presented for the rise velocity of long

Fluid	$D(\text{mm})$	$\mu(\text{mPa s})$	$\rho_l(\text{kg m}^{-3})$	$\sigma(\text{mN m})$	$U(\text{mm s}^{-1})$
Water	76.2	1.05	998	72.8	282
Silicon oil	76.2	1330	969	21.2	228
Silicon oil	76.2	3834	972	21.3	138
Water	12.7	1	1000	72	101
60% Glycerin	12.7	19	1157	68.5	101
75% Glycerin	12.7	67	1198	66.4	84

TABLE 1. The physical properties of the fluids used in the Intevap experiments.

bubbles as a function of surface tension, gravity, pipe diameter and liquid density:

$$Fr = \frac{U}{\sqrt{gD}} = \left(0.136 - 0.944 \frac{\sigma}{\rho g D^2}\right)^{1/2} \tag{15}$$

Equation (15) shows that the rise velocity decreases as the surface tension effects increase. For the particular case of negligible interfacial effects ($\sigma = 0$), equation (15) gives $Fr = 0.369$, which may be compared with the value $Fr = 0.351$ given by Dumitrescu (1943). They found excellent agreement between the theoretical solution (15) and the experimental observations.

2. Intevap experiments

The experimental set up is shown in figure 4. It consists of a transparent round acrylic pipe column with an inside diameter of 76.2 mm and a total height of 2.5 m. The tube ends at the top in an open tank. An acrylic box is connected at the column bottom. The box has a hemispherical cup held above an injection capillary tubing. This tubing is connected to a calibrated syringe as used by gas chromatographers. To obtain the desired bubble volume, the air is injected repeatedly with as many syringe strokes as necessary. The air will be trapped by the downward facing cup. The bubble is released by inverting the cup. This mechanism allowed the formation of a wide range of bubble sizes, from small (0.8 cm^3) up to Taylor bubbles (300 cm^3). A second mechanism was used to form even larger Taylor bubbles, from 300 up to 1800 cm^3 . This device replaces the transparent box. It consists of a 3 in. ball valve, a cylindrical reservoir and a drain. To form a bubble, the ball valve is closed in order to separate the liquid in the bubble formation section from the liquid in the column. Then, a desired volume of liquid is drained from the reservoir. Finally, the bubble is released by opening the valve.

To measure the rise velocity, most of the travelling bubbles were recorded with a high-speed video camera NAC HSV 1000, which acquires 500 frames per second. Due to a sudden malfunction in the HSV 1000, a Sony DXC537 video camera was also used. This camera records in NTSC video format with 30 frames per second. The frames were digitized with a PCI-1408 National Instruments image acquisition board. The image processing used the IMAQ Vision package for Labview. The video technique used for determining bubble velocities yields an error of $\pm 4\%$ for the slower bubble velocities and $\pm 2\%$ for the highest velocities.

The physical properties of the fluids used in the experiments are given in table 1.

Photographs of Taylor bubbles rising through stagnant fluid taken in these experiments are exhibited in figure 5. They have some distinctive features: (i) they are large enough to bridge the pipe and are relatively long; (ii) a film of liquid on the pipe wall terminating on the flat part of the cylindrical bubble falls under gravity;

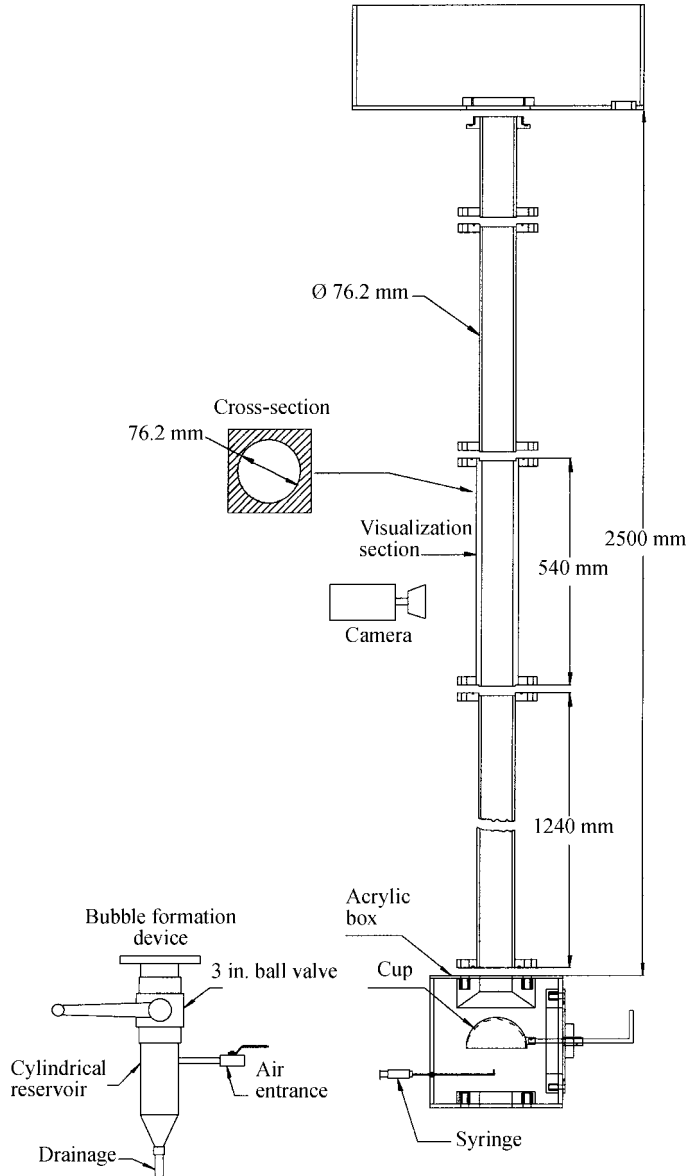


FIGURE 4. Experimental apparatus for obtaining Taylor bubbles.

(iii) the nose of the bubble is bullet shaped, nearly spherical and sharply defined; and
 (iv) the wake behind the bubble is complex and varies strongly with liquid viscosity. The wake structure is described in the caption of the cartoon shown in figure 6.

A wake type classification can be developed based on the structure of the wake observed in the photographs in figure 5. Four different types are distinguished in the cartoons in figure 7:

1. closed rounded (7a);
2. closed air cup with liquid hold up (7b, c);
3. open with wavy air membrane (7d);
4. open turbulent with bubbles detachment (7e).

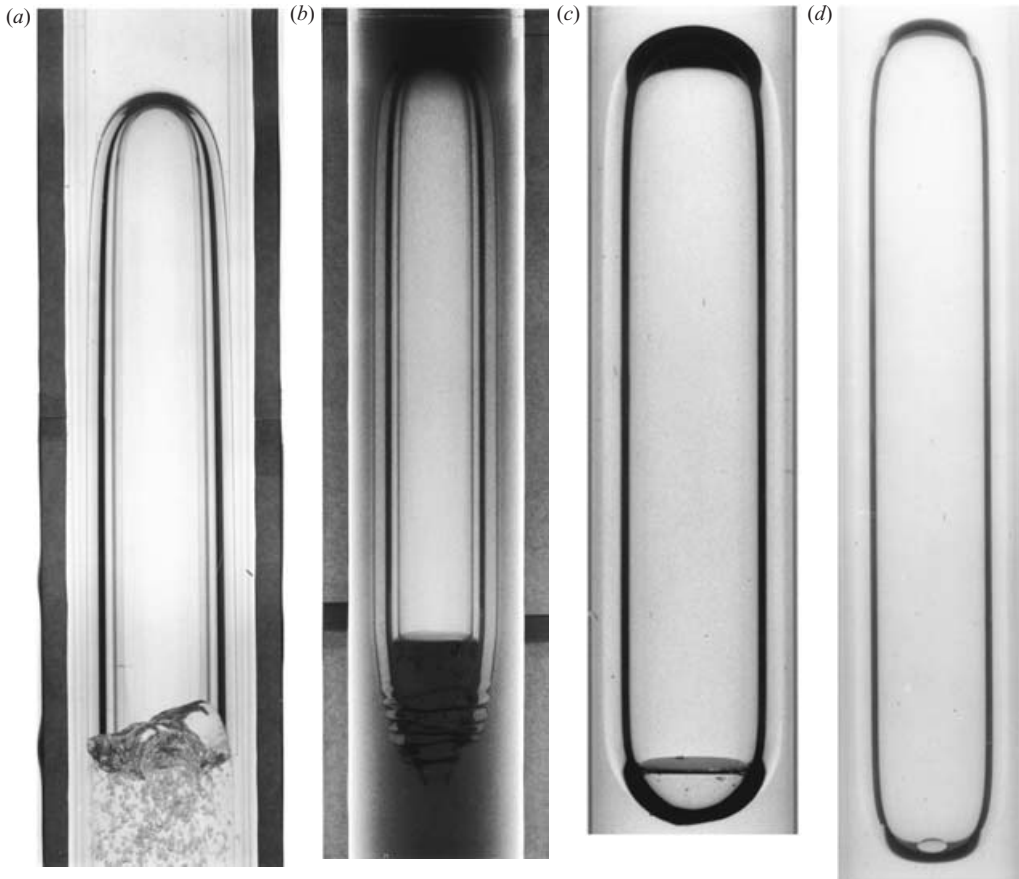


FIGURE 5. Photographs of Taylor bubbles rising through 76.2 mm inside-diameter pipe filled with different viscosity liquids: (a) water; (b) Purolub 150 oil (480 mPa s); (c) silicone oil (1300 mPa s); (d) silicone oil (3900 mPa s).

Other classifications of the wake of long gas bubbles, based on the flow pattern behind the bubble, can be found in Campos & Guedes (1988) and Pinto & Campos (1996).

Photographs of bubbles wakes of type 7(b, c, d, e) are given in figure 5(d, c, b, a). The type of wake shown in the 7(e) can be seen also in figure 1 of Pinto & Campos (1996). To our knowledge, the photograph in figure 5(b) is the only one of its type in the published literature. We expect to see rounded wakes (a) for $R < 15$, since the liquid hold up seems to decrease with R . Taylor bubbles rising in water typically have turbulent wakes but the data do not suggest that turbulence has a strong influence on the rise velocity. The influence of surface tension on the rise velocity of the bubbles shown in figure 7 can be neglected since $Eo > 40$. However, we do not know if the viscosity or the surface tension is the property that defines the shape of the wake of the bubble.

3. Processing data for power laws

We collected data on the rise velocity of Taylor bubbles from all available sources and from our own experiments at PDVSA Intevep S.A. The primitive data were

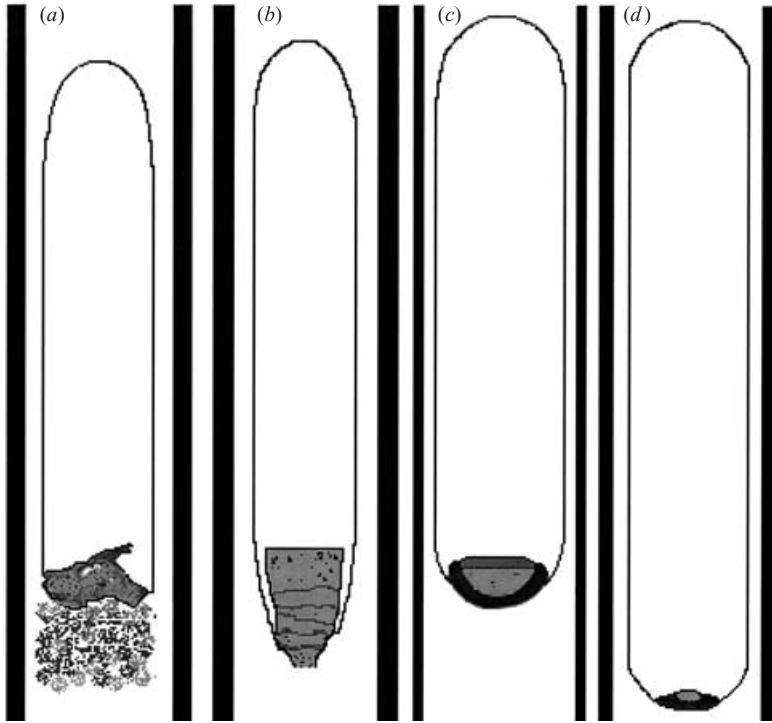


FIGURE 6. Cartoons of the Taylor bubbles shown in figure 5 which highlight great differences in the structure of the wake as the viscosity increases. (a) A bubble rising in water. A highly turbulent region with small bubbles may be observed in the wake. The bottom of this Taylor bubble is irregular and unsteady. A fast falling film drags air into the bubble's wake, which breaks up into many small bubbles that either re-enter the main bubble or are left behind. (b) A Taylor bubble in 480 mPa s machinery oil. The top is similar to that found in water; the bottom is flat and steady. The flat bottom is encapsulated by a thin wavy air membrane that surrounds the liquid at the bubble bottom. Small bubbles may be entrained into the encapsulated region. This membrane sometimes breaks into small bubbles, which are reabsorbed by the Taylor bubble. Almost none of these small bubbles are left behind the Taylor bubble. (c, d) A bubble rising through silicon oil with viscosity 1300 and 3900 mPa s respectively. The bottom of these bubbles is convex and is surrounded by an hemispherical air membrane that encapsulates some liquid and acts like a virtual 'cup' made of air holding up a small mass of liquid. No bubbles are left behind the Taylor bubble. The quantity of liquid trapped in the bubble tail is lower when the viscosity is higher (d).

processed with Mathematica 4.1 from Wolfram Research. This data is given in the Appendix in tables A1 and A2. The primitive variables were then used to form columns of dimensionless velocity, buoyancy Reynolds number and Eötvös number which we plotted systematically in log–log plots. This processing led to the universal correlation in (23) below.

Data from 262 experiments are plotted in a log Fr vs. log R plane with Eo as a parameter in figure 8. It is clear from figure 8 that the data sort into a flat region for large R (>200), a slope region for small R (<10) and a transition region between. These data are sorted in Eo groups in figure 9. Data for 19 experiments with $Eo < 6$ are plotted in the same log–log graph in figure 9(f). The scatter is much greater when Eo is less than 6 and these 19 points have not been included in the development of (23). These points are principally those in small diameter tubes in which bubbles do not move. White & Beardmore (1962) said that bubbles will not rise when

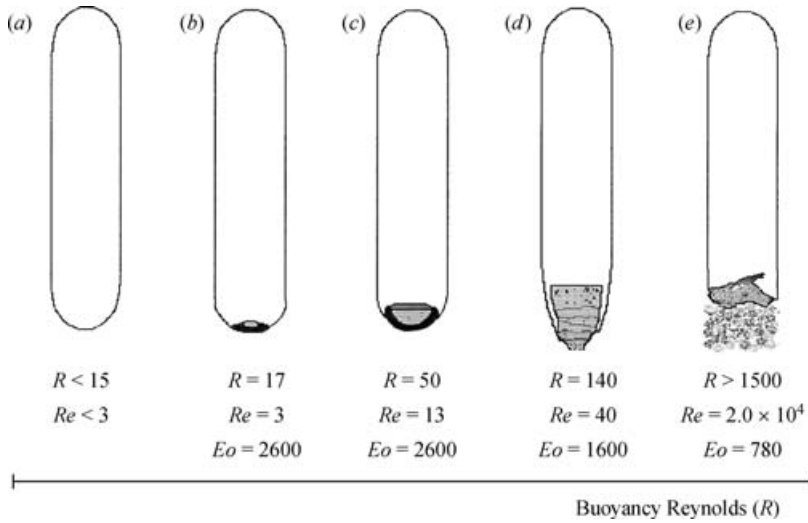


FIGURE 7. Wake types based on the structure of the wake at the tail of long gas bubbles rising in liquids sorted by the value of the buoyancy Reynolds number (R). Typical values of the Reynolds numbers ($Re = \rho g D / \mu$) and Eötvös numbers (Eo) are also shown; the flow in the wake does not seem to be turbulent in cases (a–d).

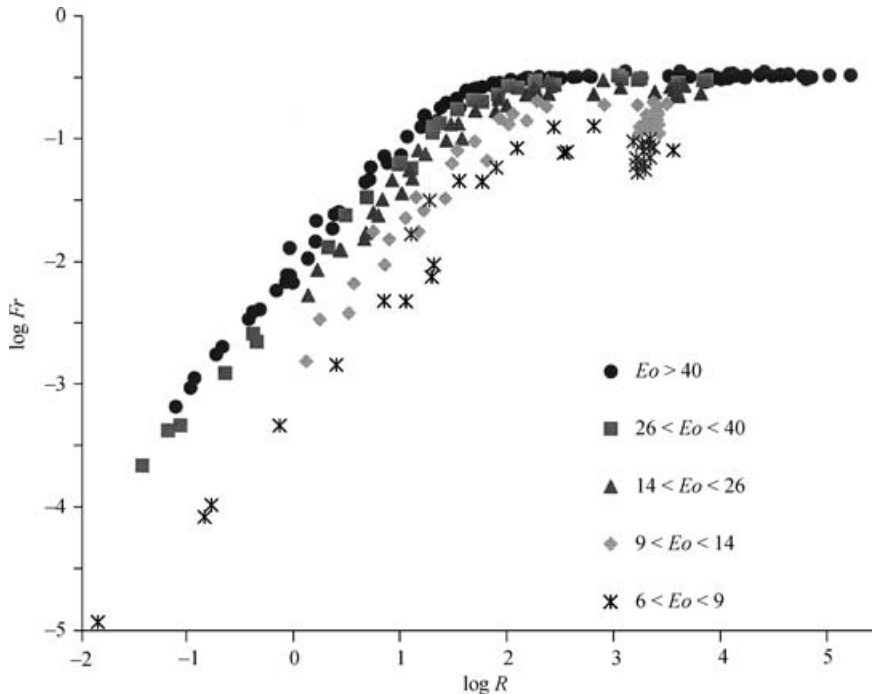


FIGURE 8. Data from all sources (with $Eo \geq 6$). Data with $Eo < 6$ are plotted in figure 9(f).

$Eo < 4$. They compared this critical $Eo = 4$ to the values 3.36 given by Hattori (1935), 3.37 given by Bretherton (1961), 0.58 given by Barr (1926) and 4 given by Gibson (1913). When the surface tension is large, the bubble tends to ball up and fill the tube.

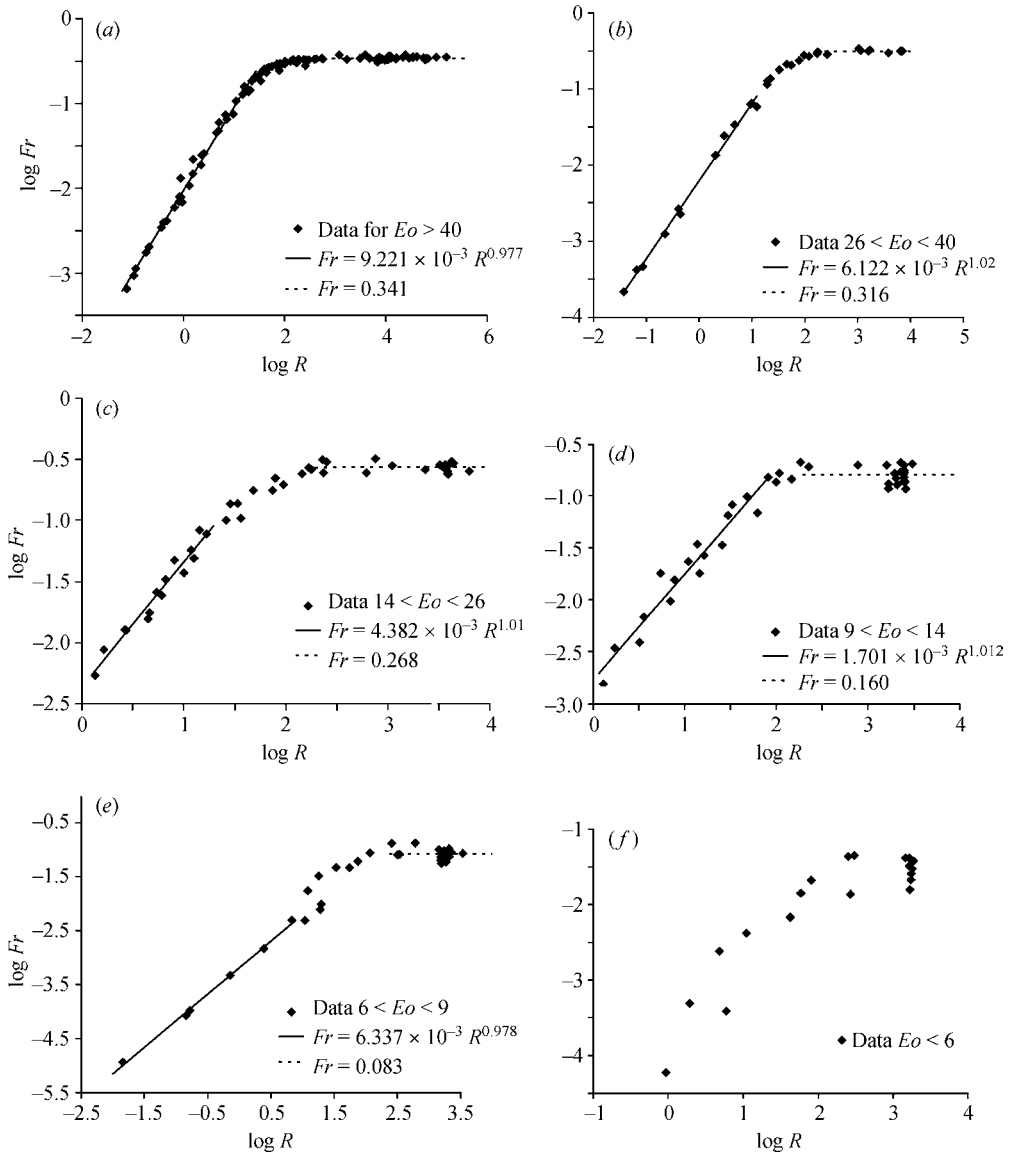


FIGURE 9. Data from figure 8 divided into various ranges of Eo : (a) $Eo > 40$, (b) $26 < Eo < 40$, (c) $14 < Eo < 26$, (d) $9 < Eo < 14$, (e) $6 < Eo < 9$, (f) $Eo < 6$. A specific power law was fitted for the slope and flat regions in each group of Eo , except for $Eo < 6$ where too much scatter is present. As can be seen from (a)–(e), the slope region has almost the same value for the slope (exponent of R), being nearly 1. This allows us to choose a single value for the exponent of the slope region regardless of Eo to develop the correlation (22) for $R < 10$.

4. Correlation construction

The plots in figure 9 show that power laws of the type $Fr = \alpha(Eo)R^{\beta(Eo)}$ can be used to collapse data on the rise velocity of long bubbles in round tubes. Typically there is a large and small buoyancy Reynolds number power law separated by transition regions which may also be processed using logistic dose curve fitting for composite correlations in the form of rational fractions of power laws.

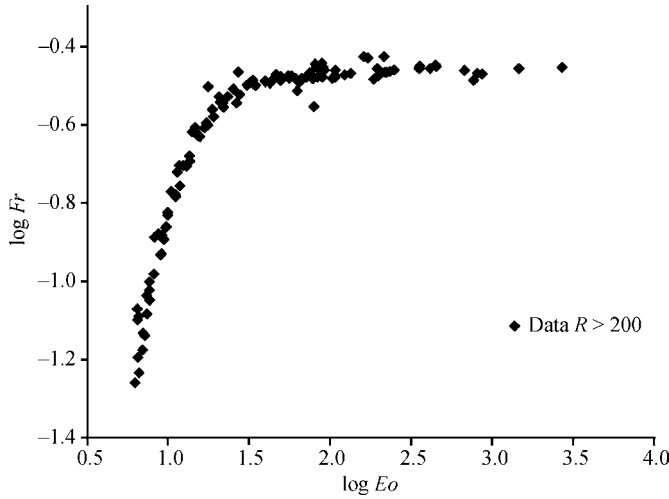


FIGURE 10. Fr vs. Eo for $R > 200$, which shows two regimes connected by a transition. For Eo large enough, say 40, the rise velocity becomes independent of surface tension effects.

4.1. Flat region: $R > 200$

To obtain the correlation (23) we took advantage of the fact that for $R > 200$, the dimensionless velocity Fr varies only with Eo (see figure 10).

For $Eo > 40$, Fr can be considered a constant:

$$Fr = 0.34, \quad Eo > 40. \tag{16}$$

This result agrees with Dumitrescu and White & Beardmore. Wallis denotes this region as inertial where liquid viscosity and surface tension are not important, but with different limits: $R > 300$ and $Eo > 100$. For White & Beardmore these limits are $R > 550$ and $Eo > 70$.

The slope region of figure 10 can be fitted with a power law:

$$Fr = 2.431 \times 10^{-3} Eo^{1.783} \quad (6 < Eo \leq 40). \tag{17}$$

Equation (17) describes the bubble’s motion only in terms of Eo . This slope region is dominated by surface tension. Wallis recognizes a similar condition but only if the bubble does not move at all with $Eo = 3.37$. White & Beardmore also describe a region where Fr is a function of Eo only for $R > 550$ and $Eo < 70$.

Logistic dose curves are a curve fitting algorithm which is well suited to describing regions of transition between power laws as the case shown in figure 10 (see Appendix by R. D. Barree in Patankar *et al.* 2002). In the present case we have

$$Fr = L[Eo; b, t, c, d] \equiv \frac{b}{\left(1 + \left(\frac{Eo}{t}\right)^c\right)^d}, \tag{18}$$

where, for figure 10:

$b = 0.34$ is the best fit constant for the flat region,

$c \times d = -1.783$ is the negative of the slope of the power law for the slope region (17),

c defines the sharpness of curvature in the transition region,

t defines the value of the independent variable (Eo) at the transition point.

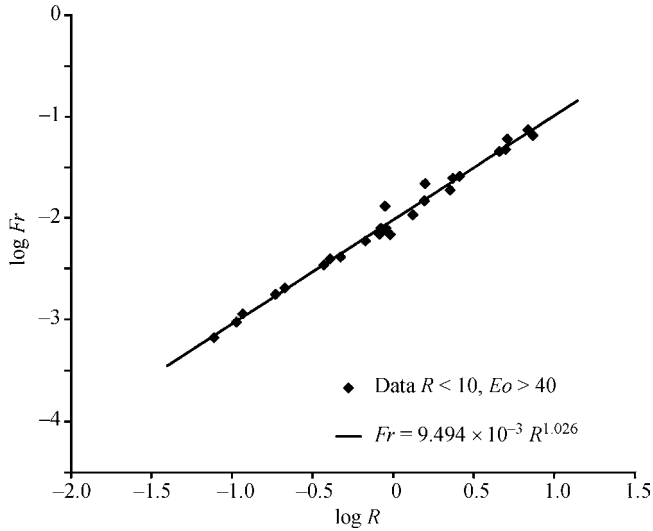


FIGURE 11. Data in the slope region with $Eo > 40$. A power law was fitted to this data. The slope for this line is applied to the rest of the data ($Eo < 40$).

We used the nonlinear regression functions of Mathematica 4.1 to obtain appropriate values for the remaining unknown parameters of (18): c , d and t . The result of this fitting is

$$Fr = \frac{0.34}{\left(1 + \frac{3805}{Eo^{3.06}}\right)^{0.58}} \tag{19}$$

4.2. Slope region: $R < 10$

The slope region is more complicated than the flat region ($R > 200$). Here, two subregions are identified for data above and below $Eo = 40$. When $Eo > 40$, Fr is a function of R alone; the data may be fitted to a power law (see figure 11).

$$Fr = 9.494 \times 10^{-3} R^{1.026}. \tag{20}$$

In figure 12, we plot all the data in the slope region with variables $Fr/R^{1.206}$ vs. Eo . Two subregions may be identified: a flat region for $Eo > 40$ and a slope region for $Eo < 40$.

A power law corresponding to the slope region of figure 12 is given by

$$\frac{Fr}{R^{1.026}} = 4.417 \times 10^{-5} Eo^{1.484}. \tag{21}$$

The power laws (20) and (21) are connected by a transition region. A composite expression in the form of a rational fraction of power laws,

$$Fr = \frac{9.494 \times 10^{-3}}{(1 + 6197/Eo^{2.561})^{0.5793}} R^{1.026}, \tag{22}$$

was obtained by processing the data with a logistic dose curve. This completes the analysis for the data with $R < 10$.

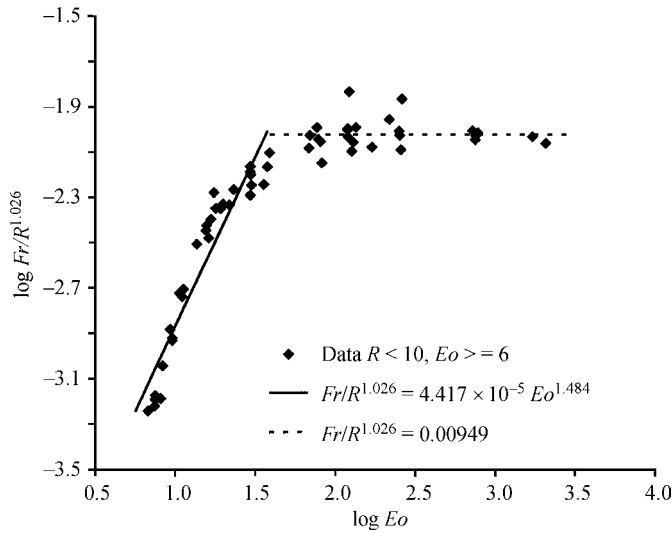


FIGURE 12. Slope region data showing the existence of two regions described by equations (20) and (21).

4.3. Universal correlation

The composite correlations for large and small R may now be joined by processing the correlations (19) and (22) with the logistic dose curve (18). This give rise to an overall universal correlation:

$$Fr = L[R; A, B, C, G] \equiv \frac{A}{\left(1 + \left(\frac{R}{B}\right)^c\right)^G}, \tag{23}$$

where

$$A = L[EO; a, b, c, d], \quad B = L[EO; e, f, g, h], \quad C = L[EO; i, j, k, l], \quad G = m/C,$$

and the parameters (a, b, \dots, l) are:

$$a = 0.34; \quad b = 14.793; \quad c = -3.06; \quad d = 0.58; \quad e = 31.08; \quad f = 29.868; \quad g = -1.96; \\ h = -0.49; \quad i = -1.45; \quad j = 24.867; \quad k = -9.93; \quad l = -0.094; \quad m = -1.0295.$$

The elaborate function given by (23) describes all of the experimental data with $EO > 6$.

The performance of the universal correlation (23) is evaluated in figures 13 and 14. In figure 13 the values predicted by (23) are compared to the experiments. Almost all of the values fall within the 20% error line and most of the data are within 10% of the predicted values. This can be seen also in figure 14(b). The sum of squared residuals is 0.03.

At this point, we wish to focus attention on the fact that (23) arises from the double application of logistic dose curve fittings. The first application leads to rational fractions of power laws which describe the EO family of curves shown in figure 15. These composite expressions can be regarded as objects which can again be processed by logistic dose curve fittings leading to the universal expression (23) in which the variations of the composite expressions shown graphically are collapsed into one

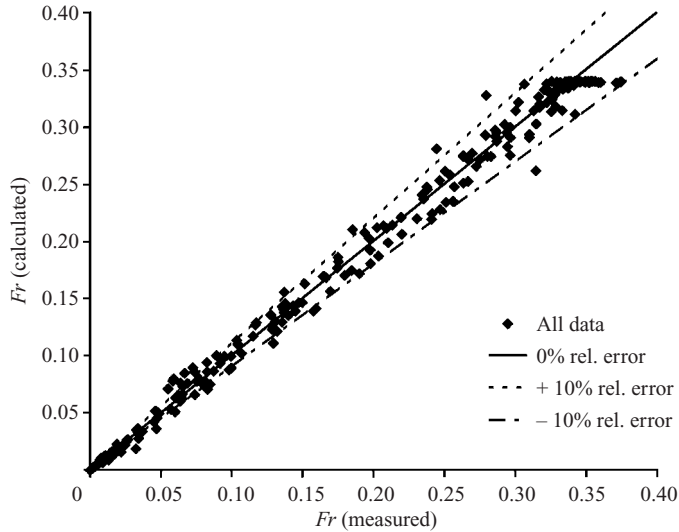


FIGURE 13. Fr predicted from (23) vs. experimental data ($EO > 6$).

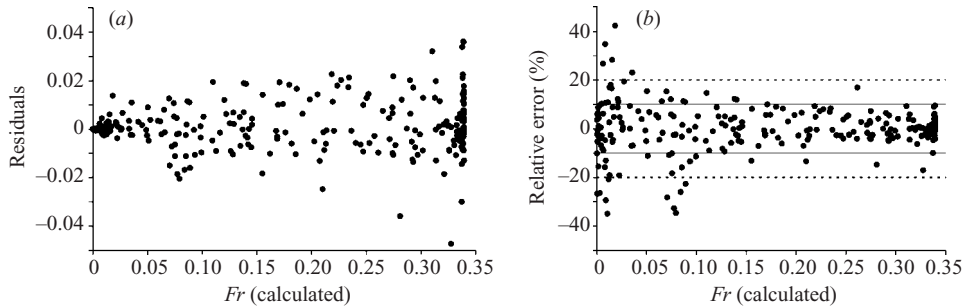


FIGURE 14. (a) Residuals plot for the universal correlation (23). This plot shows that Fr can be predicted with an error of ± 0.05 at most, (b) Relative error plot. The fitting is better at higher Fr values. This is a consequence of using the least-squares method to fit the data.

analytical expression. This procedure is a notable example of the value of systematic processing of real data for mathematical formulas describing system response.

5. Summary

The rise velocity of Taylor bubbles in round tubes was obtained by processing data for power laws. The data sorts into two different power laws for large and small buoyancy Reynolds numbers which are connected by a transition region. These curves may be described by rational functions of power laws obtained by fitting data to logistic dose curves sorted into packets depending on EO as in figure 15. A second application of dose curve fitting to the family of curves in figure 15 leads to the universal composite correlation (23) in which all experimental data are described by one universal mathematical expression.

Correlations for different regimes involving effects of inertia, interfacial tension and viscosity can be identified and associated with values of EO and R as is done in table 2.

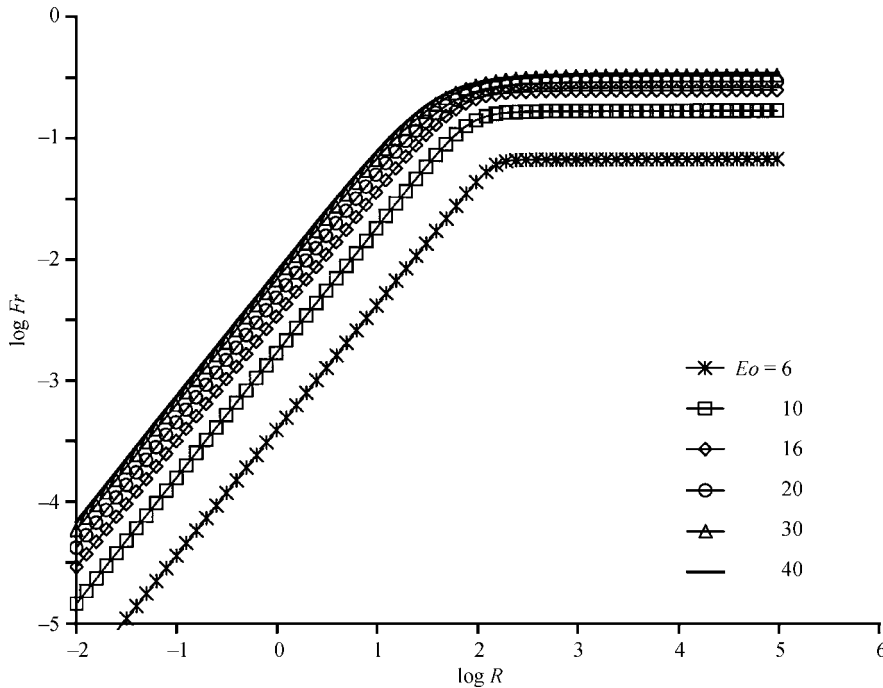


FIGURE 15. Universal correlation plot for $Eo = 6, 10, 16, 20, 30$ and 40 .

Important dimensionless parameters	Limits	Retarding forces other than inertia	Equation
Fr	$R > 200$ and $Eo > 40$	None	16
Fr, Eo	$R > 200$ and $6 < Eo < 40$	Interfacial	17
Fr, R	$R < 10$ and $Eo > 40$	Viscous	20
Fr, R, Eo	$R < 10$ and $6 < Eo < 40$	Viscous and interfacial	21
Fr, R, Eo	All data	Viscous and interfacial	23

TABLE 2. Classification of the correlations with values of dimensionless parameters.

The universal composite correlation (23) can be compared with other predictions in the literature. The graphical correlations of White & Beardmore (1962) and Zukoski (1966) were converted into formulas to facilitate the evaluation and comparison of their results with others. White & Beardmore's correlation represented the data reasonably well, with small errors for most of the data but large and erratic errors for some data. The general correlation of Wallis (1969), the analytical version of Zukoski's correlation and the universal correlation (23) all represent the data with only small errors, with a somewhat better performance for (23).

The ubiquitous tendency of natural phenomenon to follow hidden laws of self similarity is realized in the widespread success of power laws in describing experimental data. A fine collection of examples showing that '... power laws, with integer or fractional exponents, are one of the most fertile fields and abundant sources of self-similarity.', can be found in Chapter 4 of Schroeder (1990). An excellent mathematical theory of self-similarity with extensions to 'incomplete self-similarity' in which the prefactors and exponents of power laws depend on other parameters

has been developed by Barenblatt (1996). The flow of dispersed matter is a branch of fluid mechanics in which self-similarity, power laws, are widespread and widely applicable.

In this paper, we have extended the systematic processing of data for power laws to cases in which different power laws are joined by a transition region which may be described by rational fractions of power laws obtained empirically by fitting parameters of logistic dose curves. Going further, we combined the rational fraction compositions of power laws which depend on Eo (see figure 15) into an overall universal correlation (23) by fitting curves rather than points to a logistic dose curve.

6. Discussion

The correlations obtained in this paper can in some sense be regarded as the solution of the problem of determining a mathematical description of the rise velocity of long bubbles in round tubes. The accurate prediction of the rise velocity which emerges from processing data does not explain anomalous features which arise in attempting to understand the rise from the principles of fluid mechanics. Some of the anomalies which are so far not explained are:

(i) The rise velocity can be predicted without any dynamic force balance from the shape of the bubble alone.

(ii) The rise velocity is independent of the length of the bubble for long bubbles. The usual ideas based on buoyancy and Archimedes principle do not seem to apply in any obvious way.

(iii) The rise velocity does not depend on how the gas is introduced. In the Davies & Taylor (1950) experiments, the bubble column is open to the air at the bottom. In other experiments the gas is injected into a column with a closed bottom.

(iv) The predicted rise velocity is independent of the gas or liquid density or viscosity.

In Davies & Taylor (1950), the rise velocity of long gas bubbles and the spherical cap bubble, which was also analyzed by them, is determined only from the shape of the nose of the bubble and ideas from the irrotational flow of an inviscid fluid. They find for the spherical cap bubble that

$$U = K \sqrt{gD}, \quad K = \frac{\sqrt{2}}{3}, \quad (24)$$

where K is a shape factor. Batchelor (1967) notes that ‘... the remarkable feature of [equations like (24)] and its various extensions is that the speed of movement of the bubble is derived in terms of the bubble shape, without any need for consideration of the mechanism of the retarding force which balances the effect of the buoyancy force on a bubble in steady motion. That retarding force is evidently independent of Reynolds number, and the rate of dissipation of mechanical energy is independent of viscosity, implying that stresses due to turbulent transfer of momentum are controlling the flow pattern in the wake of the bubble.’

The rise of a Taylor bubble is similar, but slightly lower, with an empirical K of about 0.35. The formula (24) for the rise velocity is independent of the length of the bubble, and it is independent of the gas or liquid density or viscosity. In the case of long bubbles rising in tubes, the velocity can be strongly influenced by viscosity and surface tension. An explanation of the effect of viscosity due to liquid drainage at the tube wake was given by White & Beardmore (1962) and Brown (1965). In these analysis, the formula (24) remains important. The effects of viscosity on the

rise velocity of the spherical cap bubble for which liquid drainage is not a factor was recently obtained from an analysis based on the irrotational flow of a viscous fluid, which is based on the same assumptions as those used by Davies & Taylor. Joseph (2003) found that rise velocity is given by

$$\frac{U}{\sqrt{gD}} = -\frac{8}{3} \frac{\nu(1+8s)}{\sqrt{gD^3}} + \frac{\sqrt{2}}{3} \left[1 - 2s - \frac{16s\sigma}{\rho g D^2} + \frac{32\nu^2}{gD^3}(1+8s)^2 \right]^{1/2} \quad (25)$$

where $r_c = D/2$ is the radius of the cap, ρ and ν are the density and kinematic viscosity of the liquid, σ is the surface tension and $s = r''(0)/D$ is the deviation of the free surface

$$r(\theta) = r_c + \frac{1}{2} r''(0) \theta^2 = r_c(1 + s\theta^2)$$

from perfect sphericity: $r(\theta) = r_c$ near the stagnation point $\theta = 0$. The bubble nose is more pointed when $s < 0$ and more blunt when $s > 0$. A more pointed bubble increases the rise velocity; the blunter bubble rises slower.

The Davies & Taylor (1950) result (24) holds when all other effects vanish; if s alone is zero,

$$\frac{U}{\sqrt{gD}} = -\frac{8}{3} \frac{\nu}{\sqrt{gD^3}} + \frac{\sqrt{2}}{3} \left[1 + \frac{32\nu^2}{gD^3} \right]^{1/2}, \quad (26)$$

showing that viscosity slows the rise velocity. Equation (26) gives rise to a hyperbolic drag law

$$C_D = 6 + \frac{32}{\text{Re}} \quad (27)$$

which agrees with data on the rise velocity of spherical cap bubbles given by Bhaga & Weber (1981). The success of equation (27) in predicting the Bhaga & Weber data is associated with the fact that the uncompensated shear stress which would arise from computing viscous stresses from potential flow does not arise at the nose of the rising bubble, which is a stagnation point for the flow in a coordinate system in which the fluid is at rest.

This argument does not address the unsettling absence of an equation of motion for the Taylor bubble or the spherical cap bubble and the independence of the rise velocity from the volume of gas in the bubble. The suggestion of Batchelor in the citation below (24) that the retarding forces are associated with turbulent stresses in the wake is not consistent with the observations here (figure 7) and elsewhere that the rise velocity seems not to depend strongly on whether the wake is laminar or turbulent.

We are very grateful to Enrique Carios (PDVSA-Intevep) for his valuable help in the rise velocity experiments. Also, Edgar Suárez (PDVSA-Intevep) is credited here for the photographs shown in this paper. The work of D.D.J. was supported by Engineering Research Program of the Office of Basic Energy Sciences at the DOE, and under an NSF/GOALI grant from the Division of Chemical Transport Systems.

REFERENCES

- BARENBLATT, G. I. 1996 *Scaling, Self-similarity, and Intermediate Asymptotics*. Cambridge University Press.
- BATCHELOR, G. K. 1967 *An Introduction to Fluid Dynamics*, pp. 475–477. Cambridge University Press.

- BHAGA, T. & WEBER, M. 1981 Bubbles in viscous liquids: shapes, wakes and velocities. *J. Fluid Mech.* **105**, 61–85.
- BI, Q. C. & ZHAO, T. S. 2001 Taylor bubbles in miniaturized circular and noncircular channels. *Intl J. Multiphase Flow* **27**, 561–570.
- BROWN, R. A. S. 1965 The mechanics of large gas bubbles in tubes – I. Bubble velocities in stagnant liquids. *Can. J. Chem. Engng* **43**(5), 217–223.
- CAMPOS, J. B. L. M. & GUEDES DE CARVALHO, J. R. F. 1988 An experimental study of the wake of gas slugs rising in liquids. *J. Fluid Mech.* **196**, 27–37.
- CLIFT, R., GRACE, J. R. & WEBER, M. E. 1978 *Bubbles, Drops and Particles*, Chap. 2, p. 26. Academic.
- DAVIES, R. M. & TAYLOR, G. I. 1950 The mechanics of large bubbles rising through liquids in tubes. *Proc. R. Soc. Lond. A* **200**, 375–390.
- DUMITRESCU, D. T. 1943 Stromung and Einer Luftbluse in Senkrechten rohr. *Z. Angew. Math. Mech.* **23**(3), 139–149.
- FABRÉ, J. & LINÉ, A. 1992 Modeling of two-phase slug flow. *Annu. Rev. Fluid Mech.* **24**, 21–46.
- GOLDSMITH, H. L. & MASON, S. G. 1962 The movement of single large bubbles in closed vertical tubes. *J. Fluid Mech.* **10**, 42–58.
- GRIFFITH, P. & WALLIS, G. B. 1961 Two-phase slug flow. *J. Heat Transfer* **83**, 307–320.
- JOSEPH, D. D. 2003 Rise velocity of a spherical cap bubble. *J. Fluid Mech.* **488**, 213–223.
- LAIRD, A. D. & CHISHOLM, D. 1956 Pressure and forces along cylindrical bubbles in a vertical tube. *J. Ind. Engng Chem.* **48**, 1361–1364.
- NICKLIN, D. J., WILKES, J. O. & DAVIDSON, J. F. 1962 Two-phase flow in vertical tubes. *Trans. Inst. Chem. Engrs* **40**, 61–68.
- PATANKAR, N. A., JOSEPH, D. D., WANG, J., BARREE, R., CONWAY, M. & ASADI, M. 2002 Power law correlations for sediment transport in pressure driven channel flows. *Intl J. Multiphase Flow* **28** 1269–1292.
- PINTO, A. M. F. R. & CAMPOS, J. B. L. M. 1996 Coalescence of two gas slugs rising in a vertical column of fluid. *Chem. Engng Sci.* **51**, 45–54.
- RADER, D. W. 1973 Movement of gas slugs through Newtonian and non-Newtonian liquids in vertical annuli. MS thesis, Louisiana State University, Baton Rouge.
- RADER, D. W., BOURGOYNE, A. T. & WARD, R. H. 1975 Factors affecting bubble rise velocity of gas kicks. *J. Petrol. Tech.* **27**, 571–584.
- SCHROEDER, M. 1990 *Fractals, Chaos, Power Laws: Minutes from an Infinite Paradise*. W.H. Freeman and Co.
- TUNG, K. W. & PARLANG, J. Y. 1976 Note on the motion of long bubbles in closed tubes – Influence of surface tension. *Acta Mechanica* **24**, 313–317.
- VIANA, F., PARDO, R., RÖTZER, I. & GUZMÁN, N. 2001 Terminal rise velocity of various bubble sizes in a tube and an annular space through a viscous liquid. *Proc. Lacaflum 2001, 5th Latin American and Caribbean Congress of Fluid Mechanics, Caracas, Venezuela* (ed. S. Zarea), paper OAF-7.
- WALLIS, G. B. 1969 *One Dimensional Two-phase Flow*, Chaps. 9 and 10. McGraw-Hill.
- WARD, R. H. 1974 Movement of gas slugs through static liquids in large diameter annuli. MS thesis, Louisiana State University, Baton Rouge.
- WHITE, E. T. & BEARDMORE, R. H. 1962 The velocity of rise of single cylindrical air bubbles through liquids contained in vertical tubes. *Chem. Engng Sci.* **17**, 351–361.
- ZUKOSKI, E. E. 1966 Influence of viscosity, surface tension, and inclination angle on motion of long bubbles in closed tubes. *J. Fluid Mech.* **25**, 821–837.